

Seeing Topological Order and Band Inversion in Optical Diatomic Chain

Jun Jiang, Zhiwei Guo, Weiwei Zhu, Yang Long, Haitao Jiang, Jie Ren*, and Hong Chen*

MOE Key Laboratory of Advanced Micro-Structured Materials, School of Physics Science and Engineering, Tongji University, Shanghai 200092, China

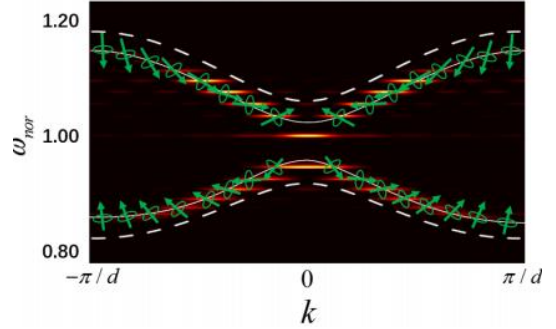
ABSTRACT: Recent realizations of exotic topological states in condensed matter and cold atoms have advanced the exploration for topological characteristics, such as invariant topological orders and band inversion. Here we construct a 1D optical diatomic system made of split ring resonators with electric-magnetic couplings to implement the topological features. We experimentally measure the dispersion relationship and sub-lattice pseudo-spin vectors by detecting field strength distributions, which determines the accompanying winding number of bulk band as the topological order. The sub-lattice pseudo-spin vector inversion observed at band-edges evidences the band inversion. We further reconfirm the band-inversion-induced topological phase transition by measuring the symmetry exchanges at band-edges. These results have shown the great potential of split ring resonator platform to experimentally explore the advanced topological characteristics, such as high winding numbers or even high Chern numbers in more exotic setups.

KEYWORDS: Topological transition, Band inversion, Winding number

Topology, as a mathematical discipline that studies invariant throughout continuous changing, has attracted much broad attention in physics since the advent of topological insulators (TIs)¹. Promising applications of TIs and relevant concepts can be found from dissipationless quantum transport² to noise-robust quantum computation³, where the nontrivial properties are characterized by the topological invariant of Bloch bands. The most well-known 2D example is the Chern number⁴, an quantized integer related to the Berry's phase⁵ crossing the Brillouin zone, which characterizes the fundamental physical phenomena of quantum (spin) Hall effect⁶⁻¹¹ and TIs. For a 1D system, such as SSH model originally introduced in an electronic context named after Su-Schrieffer-Heeger¹², the topological invariant is usually defined as winding number¹³. Though certain topological features related to winding number have been explored in crystals¹⁴ and more recently in various artificial periodic lattices for cold atoms¹⁵, acoustic waves¹⁶ or photons¹⁷, directly measurement of winding number has not yet been implemented in experiments.

Experimentally, the technical difficulties make measuring topological features in such systems remain a challenging issue, which have prompted scientists to explore other controllable platforms for analogous realizations. Moreover, in addition to measuring winding number, finding a simple method to measure topological features is significant. It is then natural to consider to observe the band-inversion and topological edge states. These phenomena, initially discussed in the context of condensed matter physics^{18, 19}, was subsequently investigated in artificial structures, such as microwave resonator chains^{20, 21}, a coupled double Peierls chain²² and quasi-1D cavities²³.

Here we construct a versatile optical platform to reveal topological features with a 1D microwave optical diatomic system, which is made of split ring resonators (SRRs) with hybrid electric-magnetic couplings²⁴. We directly measure the winding number as the topological order in this SSH-like diatomic chain to distinguish different



topological phases. In particular, we measure the bulk band dispersion and the associate pseudo-spin vectors. The band inversion is demonstrated by detecting the pseudo-spin inversion and symmetry exchange of the states at band-edges. All these results can be obtained by probing the field profile distributing over the whole chain. Although determining topological features has been experimentally explored in cold atom^{15, 25}, photonic systems^{26, 27} and acoustic systems^{16, 28} by measuring geometric phase, measuring the topological order in 1D systems, i.e., the so-called winding number, is still open and yet to be solved. In what follows, we will show how to see the winding number and band inversion in our controllable experimental platform.

EXPERIMENTAL SETUP AND ANALYTICAL MODEL.

We employ the diatomic SRR chain with alternating coupling κ_1 and κ_2 to directly measure topological order and band inversion. As depicted in Figure 1a, the chain is placed in a plane parallel waveguide whose cutoff frequency exceeds the eigenfrequencies of the system to ensure that the far-field radiation is suppressed and the near-field coupling, a key factor in tight-binding description, is dominant. An example of a unit cell, with the gaps of the two split rings are next to each other (we refer to this configuration as P1), is shown in the partial enlarged drawing in Figure 1a. Starting from configuration P1, the rings can be rotated around their centers simultaneously to mimic polyacetylenes with different topological phases¹² and six representative configurations are obtained and shown in Figure 2. In the following we will consider a general case whose unit cell is formed by a pair of arbitrarily oriented split rings (Figure 1b). The equation of motion can be approximated as follows³⁰:

$$-\omega_{nor}^2 \begin{pmatrix} a_k \\ b_k \end{pmatrix} = \begin{pmatrix} -1 & \kappa_1 + \kappa_2 e^{-ikd} \\ \kappa_1 + \kappa_2 e^{ikd} & -1 \end{pmatrix} \begin{pmatrix} a_k \\ b_k \end{pmatrix}, \quad (1)$$

where ω_{nor} denotes the frequency normalized to the resonant frequency ω_0 , $\begin{pmatrix} a_k \\ b_k \end{pmatrix}$ specifies the Bloch function of cell-periodic current states with wavevector k . It should be noted that the coupling between two SRRs is always composed of two types of coupling: magnetic and electrical coupling^{24, 29}, but one of them may be predominant in some typical configurations. When the gaps of two SRRs are next to each other (configuration P1), the dominant coupling is electrical and positive, while when gaps are exactly opposite to each other (configuration P6), the dominant coupling is magnetic and negative.

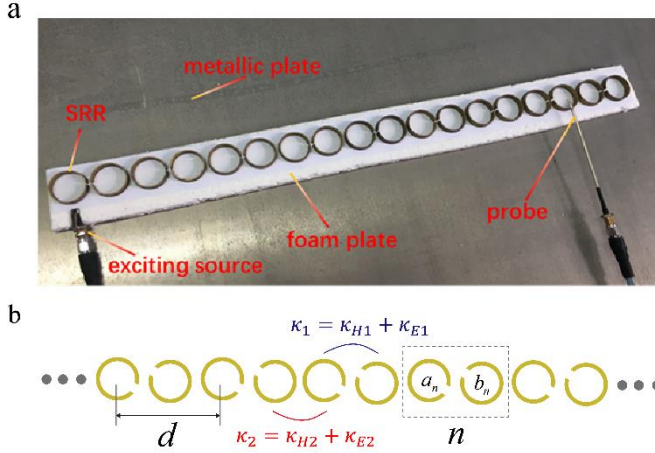


Figure 1. 1D optical SRR chain system with dimerized sites. (a) The experimental setup. The chain is composed of identical coupled copper SRRs and put on a one-centimeter-thick EPS foam plate, sandwiched between two metallic plates (note that the top plate is not shown). The two metallic plates are separated by 30mm, forming a plane parallel waveguide whose cutoff frequency is 5.0GHz. The ring dimensions are $r = 10\text{mm}$, $h = 5.0\text{mm}$, $w = 1.0\text{mm}$ and $g = 1.5\text{mm}$, the corresponding resonant frequency measured in the waveguide is $\omega_0 / 2\pi = 1.90\text{GHz}$. The chain's unit cell length is $d = 48\text{mm}$ and all rings are separated by the same center distance $d/2$. The probe connected with a network analyzer for data extraction is not shown. (b) Schematic illustration of the optical SRR chain, with A and B sublattices indicated by gap orientations. The total coupling inside the unit cell (between two unit cells) is approximately denoted by $\kappa_1 = \kappa_{H1} + \kappa_{E1}$ ($\kappa_2 = \kappa_{H2} + \kappa_{E2}$), where κ_E (κ_H) are the electrical (magnetic) couplings between two SRRs²⁴.

■ TOPOLOGICAL PHASE TRANSITION IN OPTICAL SYSTEM.

In our special system, topological phase transition can be realized by rotating all rings instead of changing their locations like others^{30, 31}. As shown in **Figure 2**, starting from P1 configuration, the trace (represented by color-coded line) of alternating coupling (κ_1 and κ_2) is plotted to demonstrate the topological phase transition as rotating all rings anticlockwise from 0 to π simultaneously. Since the bandgap would close at $|\kappa_1| = |\kappa_2|$, once the color-coded line crosses the diagonal lines indicated by $|\kappa_1| = |\kappa_2|$, the bandgap closing and re-opening process can be seen, which is a typical characteristic of topological phase transition.

For further making sure that the topological phases change, we pick six diatomic configurations with different rotation radians (rotating phases) ϕ . These configurations are denoted by P1, P2, P3,

P4, P5 and P6 and their corresponding ϕ values are 0, 0.18, 0.3, 2.85, 2.97 and π rad. Then we label the winding numbers of bulk bands and symmetries of band-edge states (the even and odd symmetry are represented by symbol '+' and '-') on their corresponding dispersion curves. The winding number of each band is obtained as³⁰:

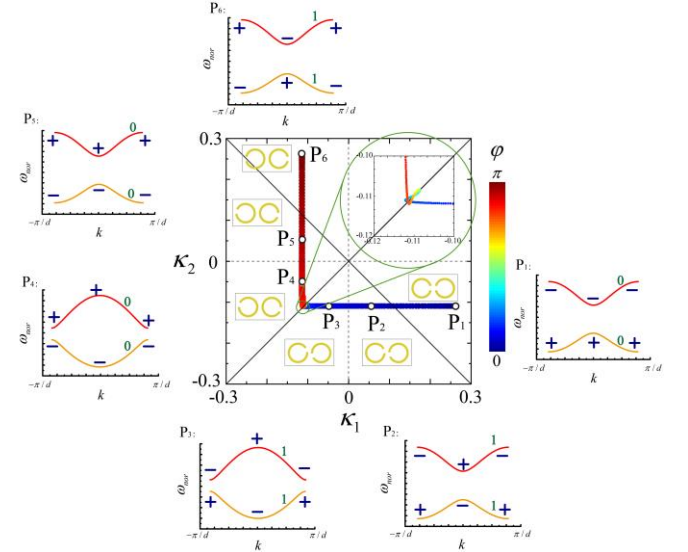


Figure 2. Topological phase transition. The color-coded line denotes the evolving phase transition in $\kappa_1 - \kappa_2$ coupling space as rotating all SRRs simultaneously anti-clockwise from two-gap face to face configuration (P1, phase 0) to two-gap-back-to-back configuration (P6, phase π). The color denotes the rotating phase as indicated by the color bar. Six representative points denoted from P1 to P6 are picked out to illustrate the topological phase transition in detail. Their corresponding unit cells and dispersion curves are plotted, together with the symmetry of band-edge state (here the symbol +/− represents even/odd symmetry) and the winding number of each band (0 or 1). Obviously, configurations P1, P4 and P5 belong to topological trivial class while other three configurations P2, P3 and P6 are topological nontrivial.

$$w_{winding} = \frac{i}{\pi} \int_{-\pi/d}^{\pi/d} \langle u_k | \partial_k | u_k \rangle dk = \frac{\theta_k}{2\pi} \Big|_{k=-\pi/d}^{k=\pi/d}, \quad (2)$$

where the normalized eigenvector $|u_k\rangle = \frac{1}{\sqrt{2}} \begin{pmatrix} e^{-i\theta_k} \\ \mp 1 \end{pmatrix}$ with

θ_k being the determined through $\tan(\theta_k) = \langle \sigma_y \rangle / \langle \sigma_x \rangle = \langle u_k | \sigma_y | u_k \rangle / \langle u_k | \sigma_x | u_k \rangle$ (σ_x and σ_y are the first and second Pauli matrix). It is obvious that if we track the point with coordinates $(\langle \sigma_x \rangle, \langle \sigma_y \rangle)$ as evolving the wave vector k through the Brillouin zone, the winding number of the corresponding bulk band can be obtained visually. The determination of symmetry of band-edge state can be readily measured from the current profile in SRRs as the field strength distribution.

From P1 to P2, the inter-intra-couplings change the order from $|\kappa_1| > |\kappa_2|$ to $|\kappa_1| < |\kappa_2|$. As a consequence, the bandgap closes and re-opens at the Brillouin zone center and the symmetries of two band-edge states at $k = 0$ exchange, similar to the band inversion process in electronic systems³²⁻³⁵. The topological transition is also indicated by the discrete change of winding numbers between 0 and 1, calculated from **Equation (2)**. From P2 to P3, merely the intracoupling κ_1 changes sign. As a result, the bands deform and the bandgap location moves from the center to the edge of the Brillouin zone, with

their winding numbers intact. From P3 to P4, the color-coded line cross the line of $\kappa_1 = \kappa_2$ backwards and forwards for several times (see the partially enlarged drawing in the inset of Figure. 2). The situations for P4 to P5 and P5 to P6 can be also discussed similarly. When directly comparing P1 and P6, it can be regarded that the topological phase transition is associated with the band inversion happens at $k = \pm\pi$ and the winding numbers switch discretely from 0 to 1.

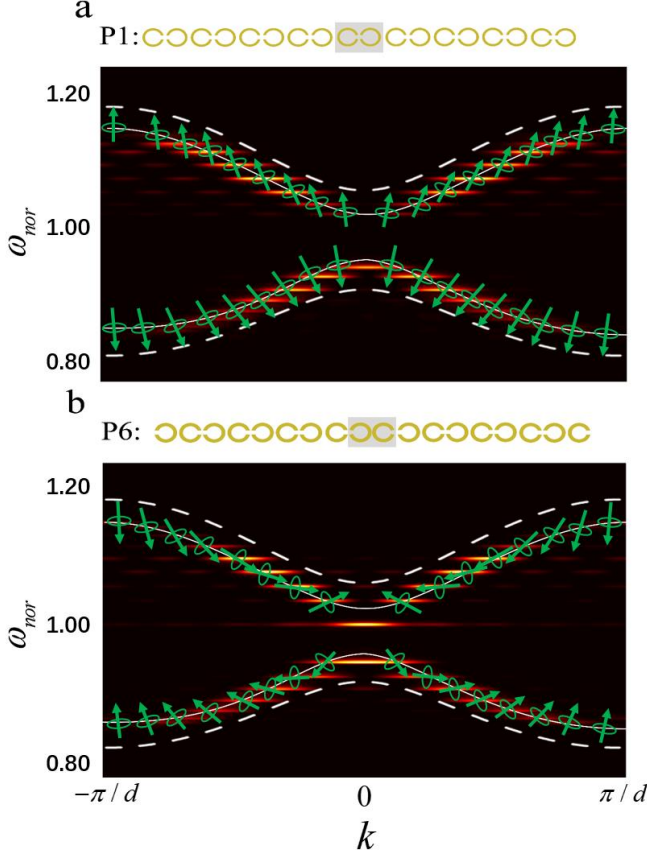


Figure 3. Measurement of the dispersions and pseudospin textures accompanying each band. (a) Dispersion diagrams $S(\omega, k)$ for P1 configuration constructed by 18 SRRs. The white dash lines denote the theoretical dispersion curves. The brighter spots are the components of the measured dispersion curves (guided by white solid lines). The sublattice pseudospin vectors are represented by the green arrows which are placed on their corresponding measured eigenmodes with the first phasor is always taken in vertical upward as the reference. (b) Dispersion diagrams $S(\omega, k)$ for P6 configuration, with experimentally measured (white solid lines), theoretically calculated dispersion curves (white dash lines) and sublattice pseudospin vectors. The existence of the midgap state is clearly observed, indicating that P6 configuration belongs to the topological non-trivial class.

MEASUREMENT OF BAND INVERSION AND WINDING NUMBERS.

The determination of 2D topological order, Chern number, has been theoretically proposed and experimentally implemented in 2D photonic crystals^{36, 37}, microwave networks³⁸, cold atoms³⁹⁻⁴². The 1D topological order, winding number, recently has also been explored experimentally in circuit QED^{43,44} and skyrmions systems⁴⁵. Our 1D optical diatom system provides alternative feasibly controllable platform, thus we follow a different scheme to determine the topological order experimentally. The topological order, that is winding number in our system, can be determined by measuring the rotating pseudospin vectors in k space directly.

Here we impose P1 and P6 chain consisting of 18 SRRs to implement the microwave measurements. The lattice sites are occupied by copper SRRs that are coupled by the evanescent near-field electromagnetic field. The tight-binding-like coupling terms κ depend on the relative orientations between two rings. The resonance frequency ω_0 of an isolated SRR is around 1.90 GHz and corresponds to the on-site energy of atoms in the tight-binding model. The experiments are performed in the frequency range of 1.50 to 2.35 GHz with a Network Analyzer connected to two probes by 50 Ohm transmission lines (the probes are both non-resonant circular loop antennas of 2mm radius with high impedance). One antenna acting as the exciting source is placed parallel with and directly below the first ring to excite the ring. The magnetic field along the chain is then detected by another probe moving along the axis of the chain at a certain distance above the rings. Though the 50-Ohm loaded probe is not matched to the analyzed structure, the detected magnetic-field signal is proportional to the current in the ring. Thus we can regard the detected signals as the flowing alternating currents.

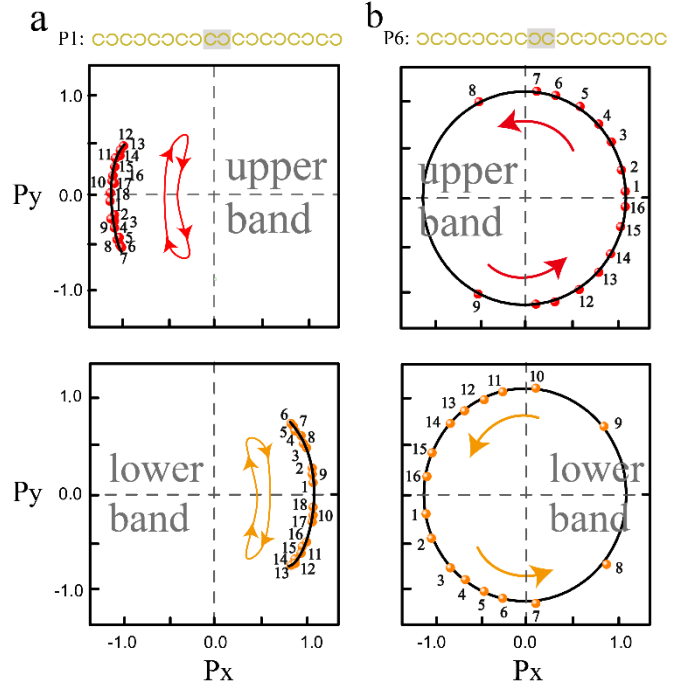


Figure 4. Measurement of the winding numbers. (a) Measurement of the components of normalized pseudospin vectors in P_x - P_y plane for the upper and lower bands of P1 configuration. The discrete balls indicate the ends of the measured pseudospin vectors. The solid black lines are the calculated results based on Eq. (5). The solid arrow lines are the eye-guided lines for the evolution path when we tune the quasi-momentum k cross the Brillouin zone from $-\pi$ to π . Obviously, the winding numbers are both zero. (b) Measurement of pseudospin vectors for upper and lower bands of the topologically nontrivial P6 configuration. The meanings of balls and lines are the same with those of (a) and the winding numbers are both one.

With the measured current in each ring, we can determine the dispersion characteristics from the spectrum function, or say, the dynamical structural factor⁴⁶

$$S(\omega, k) = \left| \sum_{n=1}^9 \left[a_{n,\omega} e^{-ikd(n-\frac{1}{2})} + b_{n,\omega} e^{-ikdn} \right] \right|^2, \quad (3)$$

where $a_{n,\omega} = I_{n,A}(\omega) e^{\varphi_{n,A}(\omega)}$, $b_{n,\omega} = I_{n,B}(\omega) e^{\varphi_{n,B}(\omega)}$ and φ_n , $X(\omega)$ (X is A or B) are amplitude and phase of the current on

the SRRs in the n th unit cell. As shown by the measured $S(\omega, k)$ in **Figure 3**, the experimental dispersion curves fitted by brighter spots are in good agreement with white dash lines based on calculated eigenfrequencies (details can be found in the part of methods). The discrete wave vectors k are acquired due to the finite short length (unit number) of the system. Nevertheless, the clear existence of midgap state in P6 band structure demonstrates that the chain configuration P6 belongs to the topological non-trivial class, consistent with the theoretical prediction.

Further, by applying discrete Fourier transform to obtain the quasi-periodic Bloch functions:

$$|u_k\rangle = \begin{pmatrix} a_k \\ b_k \end{pmatrix} = \frac{1}{C} \begin{pmatrix} \sum_{n=1}^9 a_{n,\omega} e^{-ikd(n-\frac{1}{2})} \\ \sum_{n=1}^9 b_{n,\omega} e^{-ikdn} \end{pmatrix}, \quad (4)$$

with C the normalization factor, we can obtain the two components of the pseudo-spin as [17]:

$$\begin{aligned} P_x &= \langle \sigma_x \rangle = b_k^* a_k + a_k^* b_k = \pm \cos(\theta_k) \\ P_y &= \langle \sigma_y \rangle = ib_k^* a_k - ia_k^* b_k = \pm \sin(\theta_k) \end{aligned} \quad (5)$$

We make the components of normalized pseudospin vectors in P_x - P_y plane for the upper and lower bands. As shown in **Figure 4**, the ordinal numbers are labelled beside the balls, aim to show how the pseudospin vector evolves in k space. With **Equation (2)**, the winding numbers of configuration P1 and P6 are exact 0 and 1 for both ends (upper and lower), respectively. Excellent agreement with the theoretical prediction is clearly seen. Owing to the finiteness of the short chain limited by our experiments, the distribution of the balls is not so even. Even so, it does not influence or mislead our judgement of the winding numbers acquired from distinct topological bands. We further draw all measured pseudospin vectors on the dispersion curves with the first phasor in **Figure 3a** always taken in vertical upward as the reference. Comparing **Figure 3a** (**Figure 4a**) and **Figure 3b** (**Figure 4b**), it is quite apparent that the direction of the pseudospin vectors is inverted at the edge of Brillouin zone, corresponding to the band inversion¹.

MEASUREMENT OF THE SYMMETRY OF THE BAND-EDGE STATES.

Finally, we measure the symmetry of band-edge states as a complementary evidence of the topological phase transition and band inversion⁴⁷. The eigenfrequencies at band-edge are indicated by the black vertical lines in **Figures 5a** and **5f**, which show the amplitudes of currents on the 18 SRRs for P1 and P6 chain. With the point by point measurements, the current profile distributions at band-edge frequencies can be easily obtained. Results are displayed in **Figures 5b-e** and **Figures 5g-j**. We can see that for P1 chains, the modes at band-edges share the same symmetry in both lower and upper bands, meaning that the chain is topological trivial^{28, 47}. For P6, the modes at band-edges have different symmetries in both lower and upper bands, indicating that the chain must be topological nontrivial^{29, 47}. These results agree with the measurement of winding numbers. Combining the dispersion curves of P1 and P6 chain, the measured symmetries of the current profiles at $k = \pm\pi$ are inverted: $1 \leftrightarrow 8$, $4 \leftrightarrow 5$, which also can be found in the even-odd symmetry exchange of current profiles on the central two SRRs.

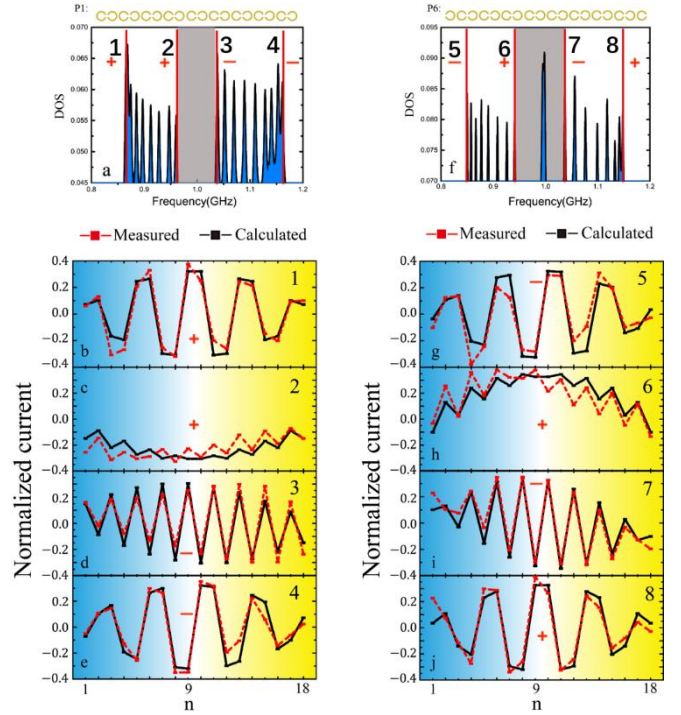


Figure 5. Measurement of the symmetry of the band-edge states. (a) Measured current spectrum on the 10th SRR for P1 chain, which is randomly selected. Measuring on other SRR does not change the current spectrum qualitatively. (b)-(e) Measured current profile as a function of site position for P1 chain at the band-edge frequencies, which are identified by the vertical lines 1-4 in (a). Red circular markers represent experimental results and black square markers represent calculated results. (f) Measured current spectrum for P6 chain. (g)-(j) Measured current spatial distribution for P6 chain at the band-edge frequencies are identified by the vertical lines 5-8 in (f). The markers + and - denote the symmetry and anti-symmetry of current profiles, respectively.

CONCLUSIONS

We have shown that a 1D periodic optical system of SRRs is an excellent platform to realize advanced concepts such as winding number, band inversion and topological midgap states. The experimental samples can be made with minimal cost and the results are intuitively easy to understand. The optical system is rather unique in the sense that Bloch states in real spaces can be measured straightforwardly and, at the same time, the Bloch states depending on wave vector k can be determined with discrete Fourier transform. As such, the global or say non-local properties can be measured locally. These attributes made it possible to straightforwardly determine the winding number of a bulk band, as well as other topology-related properties. Though all the results in this article are demonstrated in a one-dimension system, these methods have the potential to explore the relationship between the symmetry of the eigenmodes, geometrical and topological properties of bulk bands, as well as the bulk-edge correspondence in higher dimensions, which may also be useful to other applications, such as designing more complex topological artificial matters, reconstructing the geometric curvature and Bloch state Hamiltonian, and implementing topological quantum computing⁴⁸.

METHODS

Identify the symmetry of the band-edge state. The eigenvectors of **Equation (1)** for both upper and lower band are expressed as

$$|u_{k,\pm}\rangle = \begin{pmatrix} \frac{\kappa_1 + \kappa_2 \cos(kd) - i\kappa_2 \sin(kd)}{\sqrt{(\kappa_1 + \kappa_2 \cos(kd))^2 + (\kappa_2 \sin(kd))^2}} \\ \mp 1 \end{pmatrix}. \quad (6)$$

$$|u_{k,\pm}\rangle = \begin{pmatrix} e^{-i\theta_k} \\ \mp 1 \end{pmatrix}, \quad (8)$$

Because the coupling coefficient can be positive or negative in our system, we then discuss the symmetries of band-edge states in four cases: 1. $\kappa_1 > 0, \kappa_2 > 0$; 2. $\kappa_1 > 0, \kappa_2 < 0$; 3. $\kappa_1 < 0, \kappa_2 > 0$; 4. $\kappa_1 < 0, \kappa_2 < 0$. For case 1: If $|\kappa_1| > |\kappa_2|$, the chain is topological trivial.

At $k=0$, the wavefunction corresponding to the upper band

$$|u_+(k=0)\rangle = \begin{pmatrix} \frac{\kappa_1 + \kappa_2}{|\kappa_1 + \kappa_2|} \\ -1 \end{pmatrix} = \begin{pmatrix} 1 \\ -1 \end{pmatrix} \text{ is odd symmetry, while the}$$

$$\text{lower band } |u_-(k=0)\rangle = \begin{pmatrix} \frac{\kappa_1 + \kappa_2}{|\kappa_1 + \kappa_2|} \\ 1 \end{pmatrix} = \begin{pmatrix} 1 \\ 1 \end{pmatrix} \text{ is even symmetry.}$$

At $k = \pm\pi$, we get:

$$|u_+(k = \pm\pi)\rangle = \begin{pmatrix} \frac{\kappa_1 - \kappa_2}{|\kappa_1 - \kappa_2|} \\ -1 \end{pmatrix} = \begin{pmatrix} 1 \\ -1 \end{pmatrix}, \quad \text{odd symmetry;}$$

$$|u_-(k = \pm\pi)\rangle = \begin{pmatrix} \frac{\kappa_1 - \kappa_2}{|\kappa_1 - \kappa_2|} \\ 1 \end{pmatrix} = \begin{pmatrix} 1 \\ 1 \end{pmatrix}, \text{ even symmetry.}$$

If $|\kappa_1| < |\kappa_2|$, the chain is topological nontrivial.

At $k=0$, we get:

$$|u_+(k=0)\rangle = \begin{pmatrix} \frac{\kappa_1 + \kappa_2}{|\kappa_1 + \kappa_2|} \\ -1 \end{pmatrix} = \begin{pmatrix} 1 \\ -1 \end{pmatrix}, \text{ odd symmetry;}$$

$$|u_-(k=0)\rangle = \begin{pmatrix} \frac{\kappa_1 + \kappa_2}{|\kappa_1 + \kappa_2|} \\ 1 \end{pmatrix} = \begin{pmatrix} 1 \\ 1 \end{pmatrix}, \text{ even symmetry.}$$

At $k = \pm\pi$, we get:

$$|u_+(k = \pm\pi)\rangle = \begin{pmatrix} \frac{\kappa_1 - \kappa_2}{|\kappa_1 - \kappa_2|} \\ -1 \end{pmatrix} = \begin{pmatrix} -1 \\ -1 \end{pmatrix}, \quad \text{even symmetry;}$$

$$|u_-(k = \pm\pi)\rangle = \begin{pmatrix} \frac{\kappa_1 - \kappa_2}{|\kappa_1 - \kappa_2|} \\ 1 \end{pmatrix} = \begin{pmatrix} -1 \\ 1 \end{pmatrix}, \text{ odd symmetry. The other}$$

three cases can be discussed like case 1.

How to calculate and measure the winding number. The winding number is the number of loops made by a Bloch state around the equator of the Bloch sphere, as k passes through the Brillouin zone. For our model, it can be expressed as follows:

$$w_{\text{winding}} = \frac{i}{\pi} \int_{-\pi/d}^{\pi/d} (a_k^* \partial_k a_k + (b_k^* \partial_k b_k)), \quad (7)$$

Here, we rewrite Equation (6) as follows:

where θ_k is determined through $\tan(\theta_k) = \kappa_2 \sin(kd) / [\kappa_1 + \kappa_2 \cos(kd)]$. Combing Equations (7) and (8), we get

$$w_{\text{winding}} = \frac{\theta_k}{2\pi} \Big|_{k=-\pi/d}^{k=\pi/d} \quad (8)$$

By numerical calculation, the winding numbers for both upper and lower band are 1 when $|\kappa_1| < |\kappa_2|$, while they are 0 when $|\kappa_1| > |\kappa_2|$.

Though calculating the winding number is simple, measuring winding number is still a big challenge. In the following, we will give a theoretical framework about how to measure winding number. With Equations (1) and (6), we notice that

$$\begin{aligned} \kappa_1 + \kappa_2 \cos(kd) &= (b_k^* a_k + a_k^* b_k)(-\omega_{\text{nor}}^2 + 1) = \langle \sigma_x \rangle (-\omega_{\text{nor}}^2 + 1) \\ \kappa_2 \sin(kd) &= (ib_k^* a_k + ia_k^* b_k)(-\omega_{\text{nor}}^2 + 1) = \langle \sigma_y \rangle (-\omega_{\text{nor}}^2 + 1) \end{aligned} \quad (10)$$

where σ_x and σ_y are the first and second Pauli matrix. So, θ_k in

Equation (8) can be acquired by $\tan \theta_k = \langle \sigma_y \rangle / \langle \sigma_x \rangle$, which

means that if we plot these points $(\langle \sigma_x \rangle, \langle \sigma_y \rangle)$ at every wave vectors k in the equatorial plane of a Bloch sphere, the winding number of the system can be obtained visually. Usually, we employ $\langle \sigma_x \rangle$

and $\langle \sigma_y \rangle$ to represent the two components of the pseudo-spin

vectors of Bloch states and the winding number can be interpreted as the winding of the pseudo-spin vectors. All in all, the determination of the cell-periodic Bloch function of a system play a key role for measuring the winding number. For a finite chain in experiment, the cell-periodic Bloch function can be expressed as:

$$\begin{pmatrix} a_k \\ b_k \end{pmatrix} = \begin{pmatrix} \sum_{n=1} a_{n,\omega} e^{-ikd(n-\frac{1}{2})} \\ \sum_{n=1} b_{n,\omega} e^{-ikdn} \end{pmatrix}. \quad (11)$$

In our experiment, the Bloch mode $\begin{pmatrix} a_n \\ b_n \end{pmatrix}$ for both sublattices can

be determined by the directly measure (see methods section in the main text) the amplitude $I_n(\omega)$ and phase $\varphi_n(\omega)$ of currents as a function of frequency and their relationships are

$$\begin{pmatrix} a_n \\ b_n \end{pmatrix} = \begin{pmatrix} I_{n,A} e^{i\varphi_{n,A}} \\ I_{n,B} e^{i\varphi_{n,B}} \end{pmatrix}. \quad (12)$$

Measurement of spatial current distributions. In our 1D optical system containing 18 SRRs, the pseudospin vector can be determined by measuring the spatial current distribution at each eigenfrequency. The experiments were performed in the frequency range of 1.5 to 2.35GHz with a Network Analyzer connected to two probes by two 50-Ohm transmission lines (the probes are both non-resonant circular loop antennas of 2mm radius with high impedance). One antenna acted as the exciting source was placed parallel with and directly below the first ring to excite the ring. The current along the chain was then detected by another probe moving along the axis

of the chain at a certain distance above the rings. For P6 configuration, the spatial current distribution at two edge modes are not shown. The red squares represent the measured results while the black squares denote the calculated results. They are matching well. With each measured spatial current distribution, the two corresponding pseudospin vectors are labeled in green arrow lines.

AUTHOR INFORMATION

Corresponding Authors

*Email (J. Ren): Xonics@tongji.edu.cn.

*Email (H. Chen): hongchen@tongji.edu.cn.

Author Contributions

J. Jiang, J. Ren, and H. Chen conceived the idea. W. W. Zhu, H. T. Jiang, Y. Long joined discussions on the theoretical analysis. J. Jiang and Z. W. Guo performed the experimental measurements and analysis the experimental data; J. Jiang, Z. W. Guo, J. Ren, and H. Chen prepared the manuscript. All authors fully contribute to the research.

Notes

The authors declare no competing financial interest.

ACKNOWLEDGEMENTS

The authors would like to thank Dr. Paul Knott from the university of Leeds for fruitful discussions. This work is sponsored by the National Key Research Program of China (No. 2016YFA0301101), by the National Natural Science Foundation of China (NSFC) (No. 61621001), by the Natural Science Foundation of Shanghai (No. 17ZR1443800).

REFERENCES

- [1] Qi, X.L.; Zhang, S.C. Topological insulators and superconductors. *Rev. Mod. Phys.* **2011**, *83*, 1057-1110.
- [2] Murakami, S.; Nagaosa, N.; Zhang, S.C.; Dissipationless Quantum spin current at room temperature. *Science* **2003**, *301*, 1348-1351(2003).
- [3] Nayak, C.; Simon, S. H.; Stern, A.; Freedman, M.; Sarma, S. D. Non-Abelian anyons and topological quantum computation. *Rev. Mod. Phys.* **2008**, *80*, 1083-1159.
- [4] Chern, S. S. *Complex Manifolds Without Potential Theory*, Springer-Verlag, New York-Heidelberg, 1979.
- [5] Berry, M. V., Quantal phase factors accompanying adiabatic changes. *Roy. Soc. London A*. **1984**, *392*, 451.
- [6] Wang, Z.; Chong, Y. D.; Joannopoulos, J. D.; Soljačić, M. Observation of unidirectional backscattering immune topological electromagnetic states. *Nature* **2009**, *461*, 772-775.
- [7] Fang, K.; Yu, Z.; Fan, S. Realizing effective magnetic field for photons by controlling the phase of dynamic modulation. *Nat. Photon.* **2012**, *6*, 782-787.
- [8] Rechtsman, M. C.; Zeuner, J. M.; Plotnik, Y.; Lumer, Y.; Podolsky, D.; Dreisow, F.; Nolte, S.; Segev, M.; Szameit, A. Photonic Floquet topological insulators. *Nature* **2013**, *496*, 196-200.
- [9] Hafezi, M.; Demler, E. A.; Lukin, M. D.; Taylor, J. M. Robust optical delay lines with topological protection. *Nat. Phys.* **2011**, *7*, 907-912.
- [10] Khanikaev, A. B.; Mousavi, S. H.; Tse, W. K.; Kargarin, M.; MacDonald, A. H.; Shvets, G. Photonic topological insulators. *Nat. Mater.* **2013**, *12*, 233-239.
- [11] Hafezi, M.; Mittal, S.; Fan, J.; Migdall, A.; Taylor, J. M. Imaging topological edge states in silicon photonics. *Nat. Photon.* **2013**, *7*, 1001-1005.
- [12] Su, W. P.; Schrieffer, J. R.; Heeger, A. J. Solitons in polyacetylene. *Phys. Rev. Lett.* **1979**, *42*, 1698-1701.
- [13] Berge, P., Pomeau, Y. & Vidal, C. *Order within chaos*, Wiley and Sons, New York, 1984.
- [14] Callan, C. G.; Dashen, R. F.; Gross, D. J. The structure of the gauge theory vacuum. *Phys. Lett. B*. **2016**, *63*, 334-340 (1976).
- [15] Atala, M.; Aidelsburger, M.; Barreiro, J. T.; Abanin, D.; Kitagawa, T.; Demler, E.; Bloch, I. Direct measurement of the zak phase in topological Bloch bands. *Nat. Phys.* **2013**, *9*, 795-800.
- [16] Xiao, M.; Ma, G.; Yang, Z.; Sheng, P.; Zhang, Z. Q.; Chan, C. T. Geometric phase and band inversion in periodic acoustic systems. *Nat. Phys.* **2015**, *11*, 240-244.
- [17] Malzard, S.; Poli, C.; Schomerus, H. Topologically protected defect states in open photonic systems with non-hermitian charge-conjugation and parity-time symmetry. *Phys. Rev. Lett.* **2015**, *115*, 200402.
- [18] Yu, R.; Zhang, W.; Zhang, H. J.; Zhang, S. C.; Fang, Z. Quantized anomalous Hall effect in magnetic topological insulators. *Science* **2010**, *329*, 61-64.
- [19] Halperin, B. I. Quantized Hall conductance, current-carrying edge states, and the existence of extended states in a twodimensional disordered potential. *Phys. Rev. B* **1982**, *25*, 2158.
- [20] Poli, C.; Bellec, M.; Kunl, U.; Mortessagne, F.; Schomerus, H. Selective enhancement of topologically induced interface states in a dielectric resonator chain. *Nat. Commun.* **2015**, *6*, 6710.
- [21] Jiang, J.; Guo, Z. W.; Ding, Y. Q.; Sun, Y.; Li, Y. H.; Jiang, H. T.; Chen, H. Experimental demonstration of the robust edge states in a split-ring-resonator chain. *Opt. Express.* **2018**, *26*, 12891-12902.
- [22] Cheon, S.; Kim, T. H.; Lee, S. H.; Yeom, H. M. Chiral solitons in a coupled double Peierls chain. *Science* **2015**, *350*, 182-185.
- [23] Baboux, F.; Levy, E.; Lemaître, A.; Gómez, C.; Galopin, E.; Gratiot, L. L.; Sagnes, I.; Amo, A.; Bloch, J.; Akkermans, E. Measuring topological invariants from generalized edge states in polaritonic quasicrystals. *Phys. Rev. B* **2017**, *95*, 161114.
- [24] Tatartschuk, E.; Gneiding, N.; Hesmer, F.; Radkovskaya, A.; Shamonina, E.. Mapping interelement coupling in metamaterials: Scaling down to infrared. *J. Appl. Phys.* **2012**, *111*, 094904.
- [25] Jotzu, G.; Messer, M.; Desbuquois, R.; Lebrat, M.; Uehlinger, T.; Greif, D.; Esslinger, T. Experimental realization of the topological Haldane model with ultracold fermions. *Nature* **2014**, *515*, 237-240.
- [26] Zeuner, J. M.; Rechtsman, M. C.; Plotnik, Y.; Lumer, Y.; Nolte, S.; Rudner, M. S.; Segev, M.; Szameit, A. Observation of a topological transition in the bulk of a non-hermitian system. *Phys. Rev. Lett.* **2015**, *115*, 040402.
- [27] Longhi, S. Zak phase of photons in optical waveguide lattices. *Opt. Lett.* **2013**, *38*, 3716-3719.
- [28] Xiao, M.; Zhang, Z-Q.; Chan, C. T. Surface impedance and bulk band geometric phases in one-dimensional systems. *Phys. Rev. X* **2014**, *4*, 021017.
- [29] Hesmer, F. et al. Coupling mechanisms for split ring resonators: theory and experiment. *Phys. Status Solidi B* **2007**, *244*, 1170.
- [30] Blanco-Redondo, A.; Andonegui, I.; Collins, M. J.; Harari, G.; Lumer, Y.; Rechtsman, M. C.; Eggleton, B. J.; Segev, M. Topological optical waveguiding in silicon and the transition between topological and trivial defect states. *Phys. Rev. Lett.* **2016**, *116*, 163901.
- [31] Guo, Z. W.; Jiang, H. T.; Li, Y. H.; Chen, H.; Agarwal, G. S. Enhancement of electromagnetically induced transparency in metamaterials using long range coupling mediated by a hyperbolic material. *Opt. Express.* **2018**, *26*, 627-641.
- [32] King-S, R.D; Vanderbilt D. Theory of polarization of crystalline solids. *Phys. Rev. B* **1993**, *47*, 1652.
- [33] Hasan, M. Z.; Kane, C. L. Colloquium: Topological insulators. *Rev. Mod. Phys.* **2010**, *82*, 3045-3067.
- [34] Bernevig, B. A; Hughes, T.L; Zhang, S. C. Quantum spin Hall effect and topological phase transition in HgTe quantum wells. *Science* **2006**, *314*, 1757-1761.
- [35] Pankratov, O., Pakhomov, S. & Volkov, B. Supersymmetry in heterojunctions: Band-inverting contact on the basis of P b1-xSnxTe and Hg1-xCdxTe. *Solid state Comm.* **1987**, *61*, 93-96.
- [36] Skirlo, S. A.; Lu, L.; Igarashi, Y.; Yan, Q.; Joannopoulos, J.; Soljačić, M. Experimental Observation of Large Chern Numbers in Photonic Crystals. *Phys. Rev. Lett.* **2015**, *115*, 253901.
- [37] Mittal, S.; Ganeshan, S.; Fan, J.; Vaezi, A.; Hafezi, M. Measurement of topological invariants in a 2D photonic system. *Nat. Photon.* **2016**, *10*, 180-184.
- [38] Hu, W. C.; Pillay, J. C.; Wu, K.; Pasek, M.; Shum, P. P.; Chong, Y. D.. Measurement of a topological edge invariant in a microwave network. *Phys. Rev. X* **2015**, *5*, 011012.
- [39] Alba, E.; Fernandez-Gonzalvo, X.; Mur-Petit, J.; Pachos, J. K.; Garcia-Ripoll, J. J. Seeing topological order in time-of-flight measurements. *Phys. Rev. Lett.* **2011**, *107*, 235301.
- [40] Zhao, E.; Bray-Ali, N.; Williams, C. J.; Spielman, I. B.; Satija, I. I. Chern numbers hiding in time-of-flight images. *Phys. Rev. A* **2011**, *84*, 063629.
- [41] Goldman, N.; Anisimovas, E.; Gerbier, F.; Öhberg, P.; Spielman, I. B.; Juzeliūnas, J. Measuring topology in a laser-coupled honeycomb lattice: From Chern insulators to topological semimetals. *New J. Phys.* **2013**, *15*, 013025.
- [42] Aidelsburger, M.; Lohse, M.; Schweizer, C.; Atala, M.; Barreiro, J. T.; Naschimbène, S.; Cooper, N. R.; Bloch, I.; Goldman, N. Measuring the Chern number of Hofstadter bands with ultracold bosonic atoms. *Nat. Phys.* **2015**, *11*, 162-166.
- [43] Rudner, M.S.; Levitov, L.S. Topological Transition in a NonHermitian Quantum Walk. *Phys. Rev. Lett.* **2009**, *102*, 065703.

- [44] Ramasesh, V.V.; Flurin, E.; Rudner, M.; Siddiqi, I.; Yao, N. Y. Direct Probe of Topological Invariants Using Bloch Oscillating Quantum Walks. *Phys. Rev. Lett.* **2017**, *118*, 130501.
- [45] Zhang, S.L.; Laan, G.; Hesjedal, T. Direct experimental determination of the topological winding number of skyrmions in Cu₂OSeO₃. *Nat. commun.* **2017**, *8*, 14619.
- [46] Ashcroft, N. W.; Mermin, N. David. *Solid State Physics* 1976.
- [47] Zak, J. Symmetry criterion for surface states in solids. *Phys. Rev. B* **1985**, *32*, 2218-2226.
- [48] Freedman, M.H.; Kitaev, A.; Larsen, M. J.; Wang, Z. Topological quantum computation. *B. Amer. Math. Soc.* **2003**, *40*, 31-38.